Journal of
Proteomics & Bioinformatics

Jagadeesan et al., J Proteomics Bioinform 2015, 8:7
DOI: 10.4172/jpb.1000362

Research Article Open Access

Pyrazole Based Inhibitors against Enzymes of *Staphylococcus aureus*: A Computational Study

G Jagadeesan[1#], Vinodhkumar Vijayakuma[2#], Malathy Palayam[3], G Suresh[1], Gunasekaran Krishnaswamy[3], S Aravindhan[1*] and Günther H Peters[4]

[1]*Department of Physics, Presidency College, Chennai 600 005, India*
[2]*Department of Life Sciences and Chemistry, Roskilde University, 4000 Roskilde, Denmark*
[3]*CAS in Crystallography and Biophysics, University of Madras, Chennai-600025, India*
[4]*Department of Chemistry, Technical University of Denmark, 2800 Kgs. Lyngby, Denmark*
[#]*Authors contributed equally to this work*

Abstract

Pyrazole derivatives display a wide variety of biological activities such as antimicrobial, anti-inflammatory and anti-tumor activities. Its biological prominence has intrigued chemists and biologists in recent years to synthesize new pyrazole derivatives as antiviral, antibacterial and anticancer agents. The current study focuses on molecular docking and dynamics studies of pyrazole derivatives against Nucleosidase and DNA gyrase B of *Staphylococcus aureus*. Molecular docking and dynamics studies reveal that some of these derivatives show better binding abilities than some of the current drugs available on the market.

Keywords: Pyrazole derivatives; DNA gyrase B; Nucleosidase; *S.aureus*; induced fit docking; Glide; Molecular dynamics; *S.aureus* infection

Abbreviations: MTAN: Methylthioadenosine/S-adenosylhomocysteine Nucleosidase; *S.aureus: Staphylococcus aureus*; OPLSAA: Optimized Liquid Solution All Atoms

Introduction

Staphylococcus aureus (S.aureus) bacterium is involved in a wide range of diseases such as skin infections, endocarditis, meningitis, osteomyelitis, bacteremia, and sepsis. Worldwide, an estimated 2 billion people carry some form of *S.aureus*; of these, up to 53 million (2.7% of carriers) are thought to carry Methicillin-resistant *S.aureus* (MRSA) [1]. Treatment for *S.aureus* infection encountered several roadblocks due to high level of Penicillin, Vancomycin and Methicillin resistance [2]. Hence, there is a requisite for developing new anti-staphylococcal agents. The enzymes DNA gyrase B and Methylthioadenosine / S-Adenosylhomocysteine Nucleosidase (MTAN) are present in bacteria and absent in humans thereby acting as a potential target in treating the *S.aureus* related diseases.

DNA gyrase is a type II topoisomerase that catalyzes the negative supercoiling of DNA in prokaryotes. It supercoils DNA through a process of strand breakage/resealing and DNA wrapping [3]. Its function is essential to DNA replication, transcription, and bacteriophage λ integrative recombination [4,5]. Its ability to negatively supercoil a relaxed plasmid DNA substrate is unique thus serving as a target for antimicrobial drugs.

MTAN has recently been discovered and it is involved in the quorum sensing pathway of bacteria [6]. Inhibition of MTAN prevents the catalyzing mechanism needed to produce autoinducers which is necessary for the bacterial cells to sense the presence of its population. MTAN also catalyzes the irreversible cleavage of the glycosidic bond in 5'-methylthioadenosine (MTA) and S-adenosylhomocysteine (SAH) [7]. Inhibition of MTAN leads to aggregation of MTA and SAH substrates which in turn inhibits important biological processes in bacteria like polyamine synthesis, methylation, bacterial quorum sensing and methionine recycling [8]. Hence, the absence of MTAN enzyme in mammalian species and its essential role in bacteria has implicated this as a target for antimicrobial drug design [9,10].

Pyrazole and pyrazolones ring system plays an imperative role in wide range of biological activities such as antibacterial [11,12], antifungal [13], antimalarial [14], anticonvulsant, antitumor [15] and anti-inflammatory agents [16]. It is also interesting to note that pyrazoles are reported as well-known pharmacophores in targeting many diseases and in specific a potent Cannabinoid inhibitors are designed using pyrazole scaffold [17- 20]. Several drug compounds such as Cyclooxygenase-2 (Cox-2) inhibitors [21], IL-1 synthesis inhibitors, and protein kinase inhibitors [22] have a 1(H)-phenyl pyrazole motif. Furthermore, few of the 1,5-diarylpyrazole derivatives have been used in combinatorial drugs which exhibit non-nucleoside HIV-1 reverse transcriptase inhibitory activities [23]. Here, *in-silico* studies were carried with pyrazole derivatives as possible inhibitors against DNA gyrase B and Nucleosidase of *S.aureus*.

Material and Methods

Preparation of protein systems

X-ray crystal structures of DNA gyrase B (PDB ID: 3G7B) and 5'-Methylthioadenosine/S-adenosylhomocysteine Nucleosidase [MTAN] (PDB ID: 3BL6) were retrieved from the Protein Data Bank [24]. The protein structures were prepared using the protein preparation wizard program from the Schrödinger suite in which water molecules (> 5Å radius) and small molecules present were removed from the structure.

***Corresponding author:** Aravindhan S, Department of Physics, Presidency College, Chennai 600 005, India, Tel: +91 94432 03669; E-mail: aravindhanpresidency@gmail.com

Received April 01, 2015; **Accepted** June 09, 2015; **Published** June 15, 2015

Citation: Jagadeesan G, Vijayakuma V, Palayam M, Suresh G, Krishnaswamy G, et al. (2015) Pyrazole Based Inhibitors against Enzymes of *Staphylococcus aureus*: A Computational Study. J Proteomics Bioinform 8: 142-148. doi:10.4172/jpb.1000362

Part of the preparation is that the bond orders were assigned, disulphide bonds were created and hydrogens were added to the PDB structures. Restrained impref minimization with default settings was performed on the structure with optimized potentials for liquid simulations (OPLS) 2005 force field. The resulting structures were used for protein docking.

Molecular docking

The compounds intended to be used for docking were prepared using default protocol of the Ligprep program [25] in the Schrödinger's suite 9.3. Glide 5.8 program in the Schrödinger's suite 9.3 was used for docking studies. Hierarchical series of filters to search for possible locations of the ligand in the active site region of the drug target is used by Glide (**G**rid based **LI**gand **D**ocking with **E**nergetics) [26,27]. Pyrazole compounds were docked to the target protein using the Induced Fit docking (IFD) protocol. G-score and E-model scores were used as ranking criteria for the best docked ligands. Initially, 30 geometrically possible poses per compound were segregated and used for analysis.

Molecular dynamics

Molecular dynamics (MD) simulations were performed using Desmond 3. 2 [28] incorporated into the Schrödinger suite 9.3 [29]. Each simulation was carried out for 5 nanoseconds (ns). The OPLS 2005 [30] molecular mechanics force field is used for minimization and simulation. The pose with best E-model was considered for MD simulation studies. The complexes were solvated using the Desmond protocol resulting in a cubic box of 10 × 10 ×10 nm^3. For the water molecules the simple point charge (SPC) model was used. The simulation was conducted at an ionic strength of 150 mM, which was obtained by adding sodium and chloride ions (gyrase system: 22 NaCl molecules; MTAN system: 26 NaCl molecules). Additional sodium ions were added to neutralize the systems (DNA gyrase system: 7 sodium ions; MTAN system: 10 sodium ions). Energy minimization of 1000 steps using steepest descent was carried out to release the system from its conflicting contacts. The MD simulations were performed for i) DNA gyrase complex (30916 atoms) and ii) MTAN complex (28772 atoms). SHAKE algorithm [31] was used to constrain the geometry of water molecules and hydrogen bonds. A cutoff of 9 Å was used for the short-range interactions. Electrostatic interactions were calculated using smooth particle mesh Ewald method [32]. Periodic boundary conditions were applied in *x*, *y*, and *z* directions. The *NVT* (constant number of atoms *N*, volume *V* and temperature *T*) ensemble was used for the simulations. Temperature was set to 300 K and regulated by the Noose Hover thermostat using a relaxation time of 1 pico second. A time step of 1.2 femto seconds was applied. Configurations were saved every 4.8 pico seconds. Root mean square displacement (RMSD) was calculated by fitting alpha carbons of the particular frame of interest with the structure from the first time frame. Trajectories were analyzed between 2 to 5 ns.

Results and Discussion

The three dimensional x-ray structures of DNA gyrase B (PDB ID: 3G7B) and MTAN (3BL6) of *S.aureus*, retrieved from the Protein Data Bank are shown in Figures 1 and 2 along with its active site residues. DNA gyrase B and MTAN were solved in complex with its respective inhibitors namely, Ciprofloxacin and Formycin A. These complex structures reveal essential interactions between the inhibitor and the protein and these interactions are taken as the reference for the pyrazole derivative that has been elucidated in our lab. The residues of DNA gyrase B such as Glu50, Asn54, Glu58 and Thr173 present in the ATP binding pocket are involved in ATPase activity [33]. The co-crystallized ligand are forms hydrogen bond interaction with the residues Asp81, Ser129 and Leu138 (Figure 1B) which are present within the ATP binding pocket. The ligand is also further stabilized by a number of hydrophobic contacts with the residues Ile86, Pro87, Ile102, Leu103 and the side chain of Arg86.

Similarly the residues Glu11, Ser75, Glu173, Asp196 and Phe150 frame the ribose binding site of MTAN. The co-crystallized ligand forms several hydrogen bonds with the residues of Ser75, Glu171, Glu173, Asp196 and polar backbone atoms of Ile151 and Met172. Phe150 forms

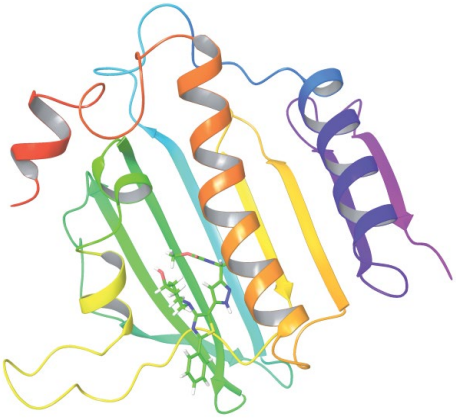

A

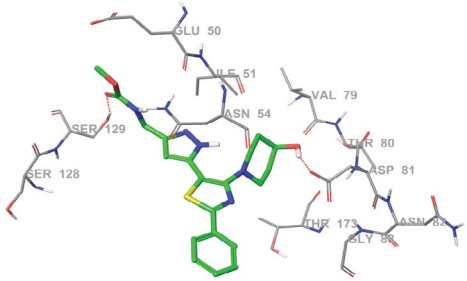

B

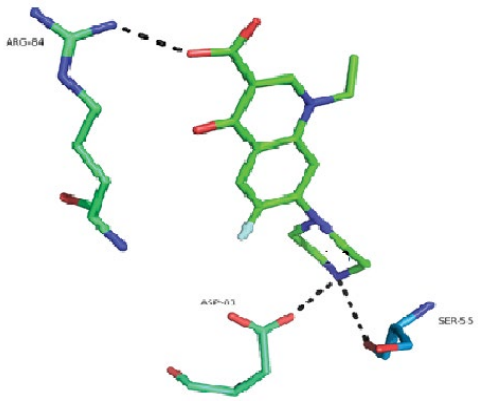

C

Figure 1: A) DNA gyrase B of *S.aureus*. B) Binding pose of crystal structure ligand (3G7B). C) Binding pose of Ciprofloxacin.

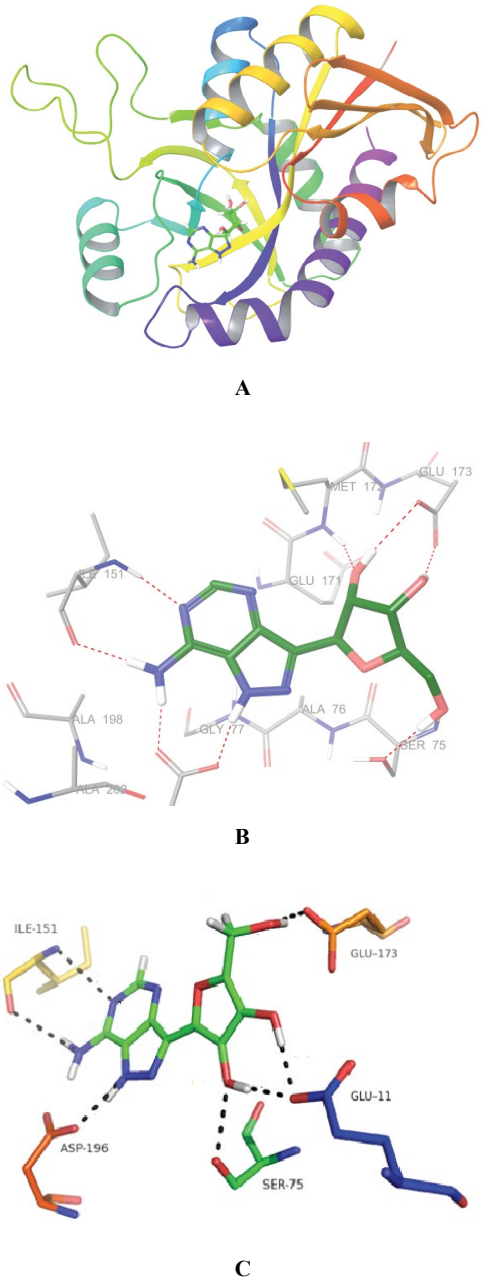

Figure 2: A) MTAN of *S.aureus* B) Binding pose of crystal structure ligand (3BL6). C) Binding pose of Formycin.

base stacking interaction with the purine ring of the co-crystallized ligand which additionally contributes to the stability of the complex. Also the residues Asp196 and Glu11 are conserved among the MTAN of other bacterial species are thought to involve in substrate binding.

The eight pyrazole derivatives shown in Figure 3 were taken for docking studies. These compounds are synthesized and their structures have been determined by X-ray crystallography [34-41]. The authors propose that these compounds could show inhibitory activity against DNA gyrase B and MTAN of *S.aureus*. The docking studies clearly reveal that some of these compounds bind efficiently to the enzymes of *S.aureus*. Glide E-model varies between -55 to -88 for compounds 1-8

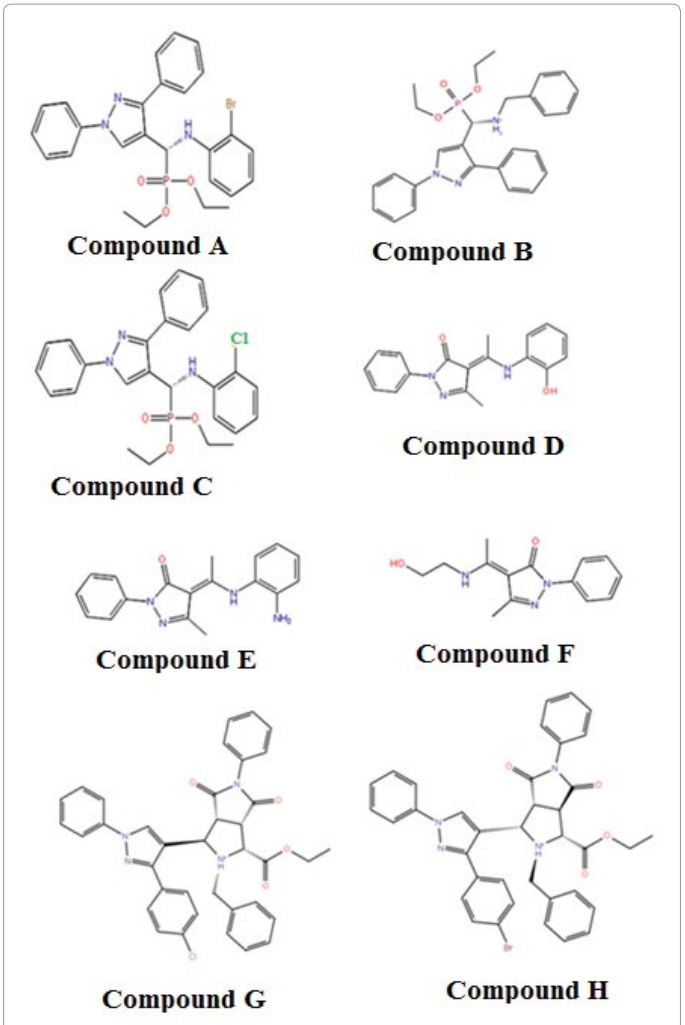

Figure 3: Schematic representation of structures of pyrazole derivatives.

tested for DNA gyrase B and -56 to -120 for MTAN (Table 1). Out of the eight pyrazole derivatives analyzed, compound A and compound H forms the best interaction with DNA gyrase B and MTAN respectively.

Interaction of the best performing pyrazole derivative with DNA gyrase B

The compound A has the highest Glide E-model score of -88.24. The oxygen atom forms hydrogen bond with the nitrogen atom of Arg84 (~3.1 Å) (Figure 4). Compound D having a Glide E-model score of -85.67, makes hydrogen bonds with the active site residue Thr173 and Asp81 of DNA gyrase B (Figure 1, Supplementary material). The oxygen atom of compound D forms a hydrogen bond with the side chain carboxylate group of Asp81 (1.94 Å) (Figure 1, Supplementary material). Compound A and D have comparable Glide E-model scores (-88.24 *vs.* -85.67). Hydrogen bond pattern are different for these two compounds. Compound A forms a hydrogen bond to Arg84 (Figure 4), whereas compound D forms hydrogen bonds with Gln58 and Asp81 (Figure 1, Supplementary material). Re-docking of the inhibitor from the co-crystallized complex structure (Figure 2, Supplementary material) of DNA gyrase B resulted in a Glide E-model score of -78.89 which is comparable to the scores found for compound A and D (Table 1). The re-docked conformation of co-crystallized ligand (Figure 2;

DNA gyrase B		
Sl.No	**Compound Name**	**Glide E-model**
1	Compound A	-88.24
2	Compound B	-73.48
3	Compound C	-63.14
4	Compound D	-85.67
5	Compound E	-55.82
6	Compound F	-72.54
7	Compound G	-72.28
8	Compound H	-76.24
9	Co-crystallized ligand (PDB ID: 3G7B)	-78.89
10	Ciproflaxin	-84.33
MTAN		
1	Compound A	-93.30
2	Compound B	-64.67
3	Compound C	-67.73
4	Compound D	-63.31
5	Compound E	-56.56
6	Compound F	-118.44
7	Compound G	-81.67
8	Compound H	-119.65
9	Co-crystallized ligand (Formycin A) (PDB ID: 3BL6)	-112.43

Table 1: Glide E-model sores of the different compounds with DNA gyrase B and MTAN of *S.aureus*.

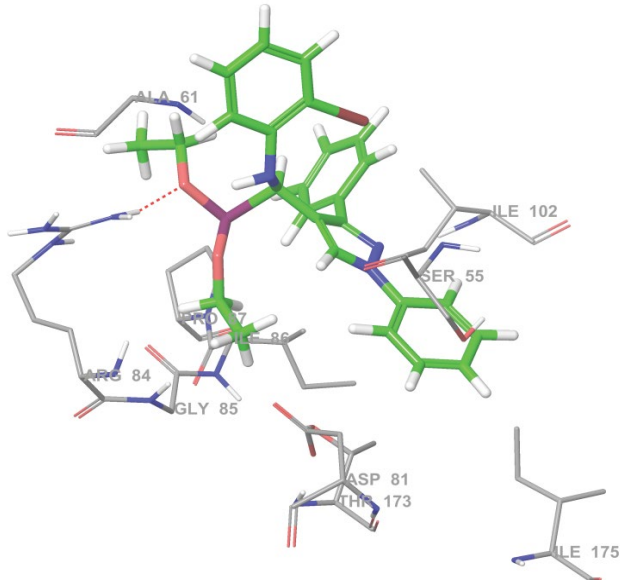

Figure 4: Interaction of best the pyrazole derivative (compound A) with DNA gyrase B of *S.aureus*.

Supplementary material) resembles the conformation of the pyrazole derivative (compound A and D respectively)

We also analyzed the interaction and energy profile of DNA gyrase B with the already available drug Ciprofloxacin [29] (Figure 3 (Supporting material)). The docking of Ciprofloxacin with DNA Gyrase B of *S.aureus* resulted in a Glide E-model score of -84.33, which is similar to the results found for compound A and D. The antibiotic showed a similar binding mode and interaction pattern as that of our pyrazole derivatives.

Interaction of the best performing pyrazole derivative with MTAN

The Compound F and H form the best interactions with MTAN of *S.aureus*. The Compound F form hydrogen bonds with Glu11, Ser75 and Arg192 of MTAN with the Glide E-model of -118.44. The compound F being small and compact binds deeper inside the active binding pocket of this enzyme with almost occupying the entire surface area of the pocket. The furan ring of the compound F forms π-π stacking interaction with the hydrophobic residue, Phe150 of MTAN. Apart from this, hydrophobic interactions are observed between the compound H - Phe206 and Compound H - Leu210 which also contributes to the stability of this complex.

On the other hand the compound H being a very big hydrophobic compound could not make any hydrophilic interaction with the defined active site residues. The MTAN - Compound H complex is mostly stabilized by hydrophobic and van der Waals interactions resulting in a Glide E-model of -119.65. Though a part of the molecule went deep into the pocket, the entry of the other half of the molecule is blocked by the presence of bulky benzene ring in the structure as indicated in Figure 5 (Phe150 and Phe206). Although the compound H has polar atoms which can accept hydrogen bonds from the receptor molecule, the presence of bromo-benzene and two other phenyl rings in the Compound H structure blocked the full entry of the molecule deep into the active site. Benzene ring in compound H displays π-π stacking with Phe-150. This π-π stacking plays a vital role in providing stability to the Compound H - MTAN complex.

In order compare the binding mode of pyrazole derivative with the already established inhibitor for this enzyme, Formycin A, a transition state analog (Figure 3, Supplementary material) is taken for docking analysis along with pyrazole derivatives. The docking results showed that our compounds also bind with the MTAN of *S.aureus* in a similar way as like the Formycin A. (E-model -112.43).

Molecular dynamics simulation

Stability of DNA gyrase – compound A and MTAN – compound H complex were evaluated through 5 ns molecular dynamics (MD)

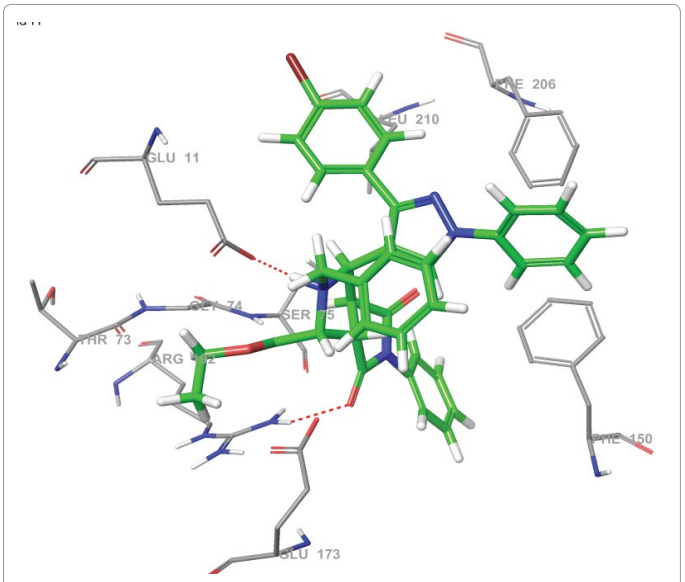

Figure 5: Interaction of best pyrazole derivative (Compound H) with MTAN of *S.aureus*.

simulations. Analysis was performed between 2 and 5ns. Root mean square displacement (RMSD) values of the DNA gyrase and MTAN Cα atoms and its respective ligands during the production phase relative to its starting structures are shown in Figure 6. Both complexes were stable, and RMSD of the Cα atoms in the proteins varied ~1Å, which is in the range commonly observed in protein simulations. The relatively large RMSD value for the compound is caused by the flipping of its benzyl ring at the start of the simulation to make π-π interactions with Phe206. The shift of ligand movement up to 4Å is due to the flipping of one benzene ring while the rest of the ligand remains in the initial position and is stabilized by hydrogen bonds. The neighboring interacting residues with compound A and H are shown in (Figure 4 and 5) (Supplementary material).

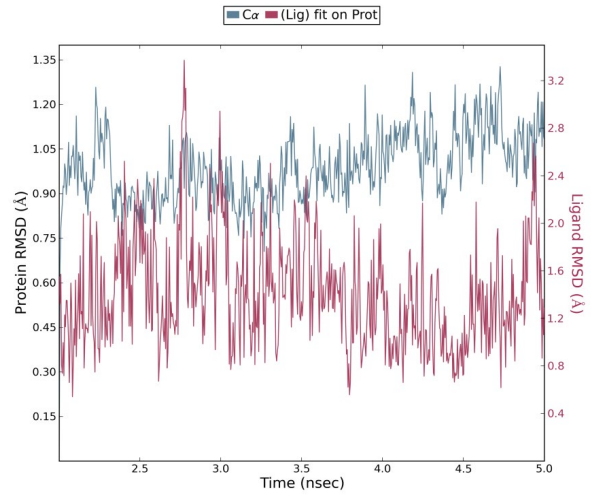

A

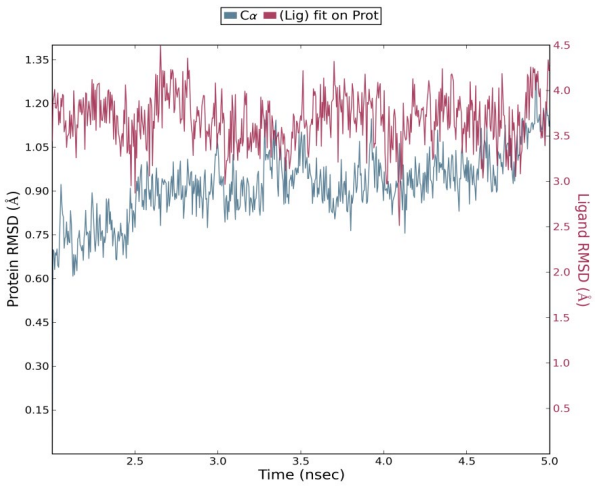

B

Figure 6: A) Root mean square displacement (RMSD) monitored during the simulation on
A) DNA gyrase B - compound A complex and
B) MTAN - compounds H complex. Protein and ligand RMSD are colored respectively blue and magenta.

Root mean square fluctuation (RMSF) is calculated for the DNA gyrase B – compound A and MTAN – compound H complexes. The RMSF is useful for characterizing local changes along the protein chain (Figure 7). Side chain fluctuations are observed within <3Å region. With few exceptions, remaining >95% of residues fluctuate within the region of 0.4 - 1.5 Å. In Figure 7 A, peaks with RMSF >1.2 Å are observed at region around Gly105, Met204 and Asn17. This is expected, since these residues are located in loop regions. In contrary, small peaks around the regions of Asn54 and Glu58 are observed indicating that there are considerable contacts during the simulation of DNA gyrase B. Glu58 maintains at least 2 contacts in the simulation (Figure 6A, Supplementary material). Glu58 maintains 52% of contacts throughout the simulation (Figure 6B, Supplementary material). Contacts between the compound and the residues Asn54 and Arg144 is established by water molecules ("water bridge") at 33% and 35% respectively (Figure 6B, Supplementary material). In the simulation on the MTAN – compound H complex, Glu11, Phe150 and Arg192 show respectively 2-3, 2 and 1 contacts throughout the simulation. Other residues which

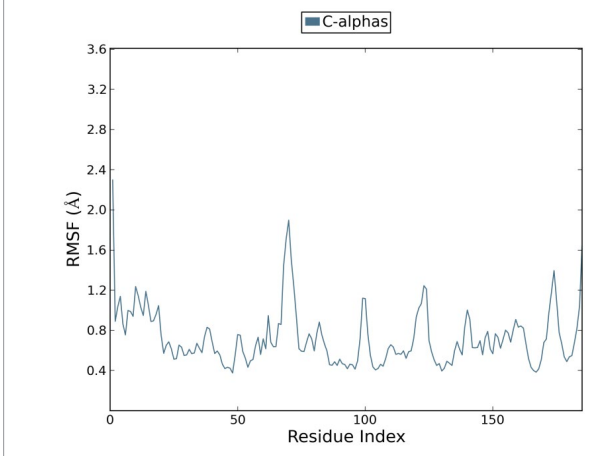

A

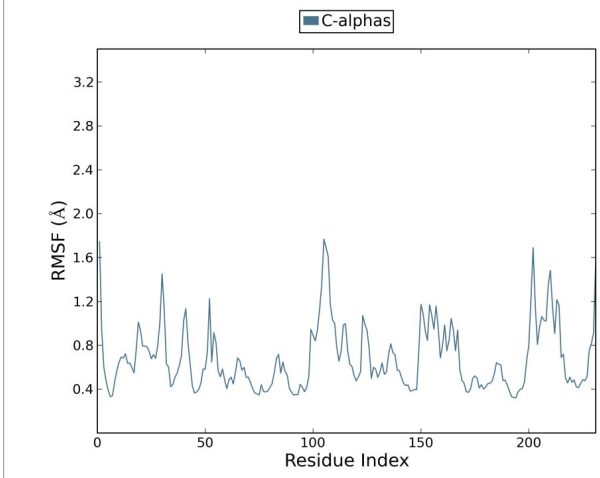

B

Figure 7: Root mean square fluctuation (RMSF) extracted from the MD simulation on
A) DNA gyrase B - compound A complex and
B) MTAN - compounds H complex.

show good contacts over a long simulation period are Phe206, Leu210 and Ile49 (Figure 7A, Supplementary material). Phe150 – compound H interactions are driven by π – π interactions. Phe150 interacts 52% and 34% of the simulation time with the benzene rings of compound H (Figure 7B, Supplementary material).

DNA gyrase – Compound A

The docking and MD simulation observed the possible residues involved in binding of Compound A to DNA gyrase. The interacting residues which were observed during IFD docking were also found replicating the interactions during simulation (Figure 8). In the above plot, we can find the hydrogen bond interaction of Glu58 (32%) and Asn54 (1.2 %) with Compound A. Since water molecules are included in the simulations, we were able to obtain this interaction through water bridge Asn54 (20 %). The hydrophobic contacts of residues Arg86 (21%), Ile102 (14 %) displayed during docking were also consistent throughout the simulation. The hydrogen bonds formed by Glu58 and Asn54 remained intact throughout the simulation (Figure 8A). We were able to observe that the residues Asn54, Gly85 and Arg144 displayed 33%, 6%, and 35% contacts with the ligand during the simulation.

MTAN – Compound H

The residues Glu11 (90%), Ser75 (18%) and Arg192 (100%) of MTAN displayed consistent hydrogen bond interactions with compound H. Residues Ser195 (17%) and Ser75 (9%) interact with the compound via water bridges. The hydrophobic interactions which is calculated for residues Ile49 (51%), Phe150 (85%), Phe206 (52%) and Leu210 (43%) are within 3.6 Å. The hydrophobic interactions of Compound H contribute the stability in the binding pocket is displayed by the π-π interaction of the benzene ring with residues Phe-150 and Phe-206 of MTAN. There are also some ionic interactions displayed by the residues Glu211 and Arg192 respectively. The residues Glu11, Phe150 and Arg192 maintain the contacts with the compound H at 100%, 52% and 90% respectively during the entire simulation.

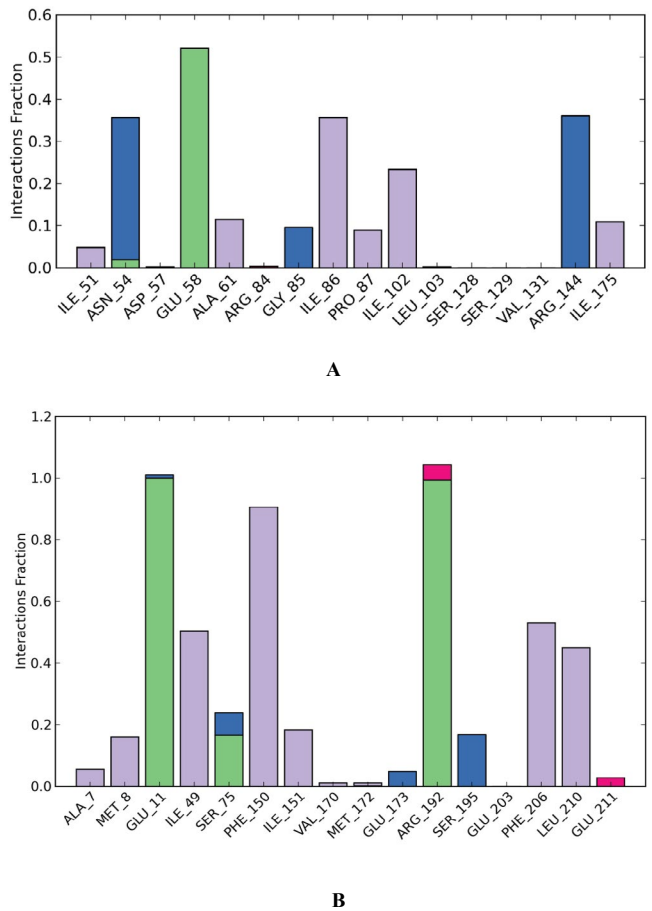

Figure 8: Protein-ligand contacts with active site residues. A) DNA gyrase B - compound A.
B) MTAN – compound H. Color coding is as follows: H-bond: green; hydrophobic interactions: violet; water bridge: blue; ionic interactions: red.

Conclusion

MTAN important for the catalysis of irreversible cleavage of the glycosidic bond in 5'-methyladenosine (MTA) and S-adenosylhomocysteine (SAH) and DNA gyrase B important for the supercoiling of DNA during replication plays a vital role in the pathogenic bacterium *S.aureus*. Docking analysis of all the eight pyrazole derivatives, two drugs Ciprofloaxcin and Formycin A as well as MD simulations of the best ligands with the protein targets, DNA gyrase B and MTAN of *S.aureus* revealed important interactions between the derivatives and enzymes. The docking studies with the structure of pyrazole derivatives show that the compound A and F being small and compact molecule are located deep into the active site of the MTAN and DNA gyrase B of *S.aureus*. On the other hand, binding of the compound H to the active site of MTAN is prevented by the presence of bulky side chains causing steric clashes.

In order to compare pyrazole derivatives for its efficiency standard drugs Ciprofloaxcin and Formycin A shown in Figure 1c and 2c is included in our docking studies. The above established enzyme-inhibitor complex is taken as a model for explaining our pyrazole derivatives interaction with the active sites of the enzyme MTAN and DNA gyrase B of *S.aureus*. MD simulations of these best compounds (compound A- DNA Gyrase B and Compound H-MTAN) help us to understand the interactions of the protein- ligand complex in a better way. From our MD results we are able to describe water bridges observed with the residues of Arg-144 in DNA gyrase complex.

Through Molecular docking and dynamics studies, it was clear that among the eight pyrazole derivatives, the compound A, D, F and H shows better binding to DNA gyrase B and MTAN of *S.aureus*. The docking studies with the pyrazole derivatives showed that our derivatives also established a similar way of binding with the target protein which is explained by their comparable binding energy and interaction with the active site residues of the enzymes. To both of the target proteins, the phenol and the pyrazole ring plays a vital role in holding the molecule in place by forming hydrogen bond with the active site residues. Thus, the newly derived pyrazole derivatives show better mode of binding than the already available inhibitor and our finding will help in designing a novel anti-staphylococcal agents.

References

1. Klevens RM, Morrison MA, Nadle J, Petit S, Gershman K, et al. (2007) Invasive methicillin-resistant Staphylococcus aureus infections in the United States. JAMA 298: 1763-1771.
2. Wang JL, Tseng SP, Hsueh PR, Hiramatsu K (2004) Vancomycin heteroresistance in methicillin-resistant Staphylococcus aureus, Taiwan. Emerg Infect Dis 10: 1702-1704.
3. Ruiz J1 (2003) Mechanisms of resistance to quinolones: target alterations, decreased accumulation and DNA gyrase protection. J Antimicrob Chemother 51: 1109-1117.

4. Sutcliffe JA, Gootz TD, Barrett JF (1989) Biochemical characteristics and physiological significance of major DNA topoisomerases. Antimicrob Agents Chemother 33: 2027-2033.

5. Advances In Protein Chemistry, Volume 38 (Google eBook). (1986) Academic Press.

6. Parveen N, Cornell KA (2011) Methylthioadenosine/S-adenosylhomocysteine nucleosidase, a critical enzyme for bacterial metabolism. Mol Microbiol 79: 7-20.

7. Siu KKW, Lee JE, Smith GD, Horvatin-Mrakovcic C, Howell PL (2008) Structure of Staphylococcus aureus 5'-methylthioadenosine/S-adenosylhomocysteine nucleosidase. Acta Crystallogr Sect F Struct Biol Cryst Commun 64: 343-350.

8. Miller JW, Nadeau MR, Smith J, Smith D, Selhub J (1994) Folate-Deficiency-Induced Homocysteinaemia In Rats: Disruption Of S-Adenosylmethionine's Co-Ordinate Regulation Of Homocysteine Metabolism. Biochem J 298: 415-419.

9. Schauder S, Shokat K, Surette MG, Bassler BL (2001) The LuxS family of bacterial autoinducers: biosynthesis of a novel quorum-sensing signal molecule. Mol Microbiol 41: 463-476.

10. Chen X, Schauder S, Potier N, Van Dorsselaer A, Pelczer I, et al. (2002) Structural identification of a bacterial quorum-sensing signal containing boron. Nature 415: 545-549.

11. Nagamallu R, Kariyappa AK (2013) Synthesis and biological evaluation of novel formyl-pyrazoles bearing coumarin moiety as potent antimicrobial and antioxidant agents. Bioorg Med Chem Lett 23: 6406-6409.

12. Deshmukh MB, Salunkhe SM, Patil DR, Anbhule PV (2009) A novel and efficient one step synthesis of 2-amino-5-cyano-6-hydroxy-4-aryl pyrimidines and their anti-bacterial activity. Eur J Med Chem 44: 2651-2654.

13. Gholap AR, Toti KS, Shirazi F, Deshpande MV, Srinivasan KV (2008) Efficient synthesis of antifungal pyrimidines via palladium catalyzed Suzuki/Sonogashira cross-coupling reaction from Biginelli ,4-dihydropyrimidin-2(1H)-ones. Tetrahedron 64: 10214-10223.

14. Azas N, Rathelot P, Djekou S, Delmas F, Gellis A, et al. (2003) Antiparasitic activity of highly conjugated pyrimidine-,4-dione derivatives. Farmaco 58: 1263-1270.

15. Ghorab MM, Ragab FA, Heiba HI, Youssef HA, El-Gazzar MG (2010) Synthesis of novel pyrrole and pyrrolo[,3-d]pyrimidine derivatives bearing sulfonamide moiety for evaluation as anticancer and radiosensitizing agents. Bioorg Med Chem Lett 20: 6316-6320.

16. Said SA, Amr Ael-G, Sabry NM, Abdalla MM (2009) Analgesic, anticonvulsant and anti-inflammatory activities of some synthesized benzodiazipine, triazolopyrimidine and bis-imide derivatives. Eur J Med Chem 44: 4787-4792.

17. Menozzi G, Fossa P, Cichero E, Spallarossa A, Ranise A, et al. (2008) Rational design, synthesis and biological evaluation of new ,5-diarylpyrazole derivatives as CB1 receptor antagonists, structurally related to rimonabant. Eur J Med Chem 43: 2627-2638.

18. Cichero E, Menozzi G, Spallarossa A, Mosti L, Fossa P (2008) Exploring the binding features of rimonabant analogues and acyclic CB1 antagonists: docking studies and QSAR analysis. J Mol Model 14: 1131-1145.

19. Pinna G, Curzu MM, Dore A, Lazzari P, Ruiu S, et al. (2014) Tricyclic pyrazoles part 7. Discovery of potent and selective dihydrothienocyclopentapyrazole derived CB2 ligands. Eur J Med Chem 85: 747-757.

20. Chang CP, Wu CH, Song JS, Chou MC, Wong YC, et al. (2013) Discovery of 1-(,4-dichlorophenyl)-N-(piperidin-1-yl)-4-((pyrrolidine-1-sulfonamido) methyl)-5-(5-((4-(trifluoromethyl)phenyl)ethynyl)thiophene-2-yl)-1H-pyrazole-3-carboxamide as a novel peripherally restricted cannabinoid-1 receptor antagonist with significant weight-loss efficacy in diet-induced obese mice. J Med Chem 56: 9920-9933.

21. Dannhardt G, Laufer S (2000) Structural approaches to explain the selectivity of COX-2 inhibitors: is there a common pharmacophore? Curr Med Chem 7: 1101-1112.

22. Pyrazole compounds useful as protein kinase inhibitors (2003) Patent Number: 6,696,452.

23. Cichero E, Fossa P (2012) Docking-based 3D-QSAR analyses of pyrazole derivatives as HIV-1 non-nucleoside reverse transcriptase inhibitors. J Mol Model 18: 1573-1582.

24. Bernstein FC, Koetzle TF, Williams GJB, Meyer EF, Brice MD, et al. (1977) The Protein Data Bank. A Computer-Based Archival File for Macromolecular Structures. J Mol Biol 112: 535-542.

25. Suite 2012: LigPrep. New York, NY, 2012: Schrödinger, LLC.

26. Halgren TA, Murphy RB, Friesner RA, Beard HS, Frye LL, et al. (2004) Glide: a new approach for rapid, accurate docking and scoring. 2. Enrichment factors in database screening. J Med Chem 47: 1750-1759.

27. Friesner RA, Banks JL, Murphy RB, Halgren TA, Klicic JJ, et al. (2004) Glide: a new approach for rapid, accurate docking and scoring. 1. Method and assessment of docking accuracy. J Med Chem 47: 1739-1749.

28. Shan Y, Kim ET, Eastwood MP, Dror RO, Seeliger MA, et al. (2011) How does a drug molecule find its target binding site? J Am Chem Soc 133: 9181-9183.

29. Suite 2012: Maestro. Suite 2012: Maestro. LLC, New York, NY, 2012: Schrödinger.

30. Kaminski GA, Friesner RA, Tirado-Rives J, Jorgensen WL (2001) Evaluation and Reparametrization of the OPLS-AA Force Field for Proteins via Comparison with Accurate Quantum Chemical Calculations on Peptides. The Journal of Physical Chemistry B 105: 6474-6487.

31. Ryckaert JP, Ciccotti G, Berendsen HJC (1977) Numerical integration of the cartesian equations of motion of a system with constraints: molecular dynamics of n-alkanes. Journal of Computational Physics 23: 327-341.

32. Essmann U, Perera L, Berkowitz ML, Darden T, Lee H, et al. (1995) A smooth particle mesh Ewald method. J Chem Phys 103: 8577-8593.

33. Gross CH, Parsons JD, Grossman TH, Charifson PS, Bellon S, et al. (2003) Active-Site Residues of Escherichia coli DNA Gyrase Required in Coupling ATP Hydrolysis to DNA Supercoiling and Amino Acid Substitutions Leading to Novobiocin Resistance. Antimicrobial Agents and Chemotherapy 47: 1037-1046.

34. Jagadeesan G, Suresh G, Nandakumar B, Perumal PT, Aravindhan S (2011) Diethyl [benzyl-amino-(,3-diphenyl-1H-pyrazol-4--yl)meth-yl]phospho-nate. Acta Crystallogr Sect E Struct Rep Online 67: o2376.

35. Jayarajan R, Sharmila P, Jagadeesan G, Vasuki G, Aravindhan S (2011) (Z)-4-{1-[(2-Hy-droxy-ethyl)-amino]-ethyl-idene}-3-methyl-1-phenyl-1H-pyrazol-5(4H)-one. Acta Crystallogr Sect E Struct Rep Online 67: o444.

36. Sharmila P, Jayarajan R, Jagadeesan G, Vasuki G, Aravindhan S (2011b) Crystal Structure of (Z)-4-(1-(2-hydroxyphenylimino)ethyl)-3-methyl-1-phenylpyrazol-5-ol. Structural Chemistry Communications.

37. Suresh G, Nandakumar A, Sabari V, Perumal PT, Aravindhan S (2013) Diethyl [(2-chloro-anilino)(,3-diphenyl-1H-pyrazol-4-yl)meth-yl]phospho-nate. Acta Crystallogr Sect E Struct Rep Online 69: o182.

38 Suresh G, Sabari V, Nandakumar A, Perumal PT, Aravindhan S (2012) Diethyl [(2-bromo-anilino)(,3-diphenyl-1H-pyrazol-4-yl)meth-yl]phospho-nate. Acta Crystallogr Sect E Struct Rep Online 68: o1554.

39. Jayarajan R, Sharmila P, Jagadeesan G, Vasuki G, Aravindhan S (2011) (Z)-4-{1-[(2-Hy-droxy-ethyl)-amino]-ethyl-idene}-3-methyl-1-phenyl-1H-pyrazol-5(4H)-one. Acta Crystallogr Sect E Struct Rep Online 67: o444.

40. Kamatchi P, Jagadeesan G, Pramesh M, Perumal PT, Aravindhan S (2012) Ethyl 2-benzyl-3-[3-(4-chloro-phen-yl)-1-phenyl-1H-pyrazol-4-yl]-,6-dioxo-5-phenyl-octa-hydro-pyrrolo-[,4-c]pyrrole-1-carboxyl-ate. Acta Crystallogr Sect E Struct Rep Online 68: o552.